A Leg Configuration Sensory System for Dynamical Body State Estimates in a Hexapod Robot*

Pei-Chun Lin§ Haldun Komsuoğlu † Daniel E. Kodistchek†
pclin@umich.edu hkomsuog@umich.edu kod@eecs.umich.edu
§Department of Mechanical Engineering, The University of Michigan, Ann Arbor
†Department of Electrical Engineering and Computer Science, The University of Michigan, Ann Arbor

Abstract

We report on a novel leg strain sensory system for the autonomous robot RHex [8] implemented upon a cheap, high performance local wireless network [1]. We introduce a model for RHex's 4-bar legs [4] relating leg strain to leg kinematic configuration in the body coordinate frame. We compare against ground truth measurement the performance of the model operating on real-time leg strain data generated under completely realistic operating conditions. We introduce an algorithm for computing six degree of freedom body posture measurements in world frame coordinates from the outputs of the six leg configuration models, together with a priori information about the ground. We discuss the manner in which such stance phase configuration estimates will be fused with other sensory data to develop the continuous time full body state estimates for RHex.

1 Introduction

The hexapedal robot, RHex [8], presently driven by task level open loop controllers performs extraordinarily well over badly broken and unstable surfaces at speeds exceeding two body lengths per second [9]. However, both the efficiency and behavioral repertoire of RHex are limited because of the lack of information about its state and that of its environment. In our initial studies with sensor based controllers we observed significant behavioral improvement from even minimal feedback [2,6]. In this paper we describe a much longer step toward the implementation of robust full state estimation for RHex.

A recently developed high performance family of dynamical hexapedal robot running controllers presumes the availability of full body state estimates [5] throughout the stance and flight phases of locomotion. This paper introduces a novel leg strain sensory system for the autonomous robot RHex [8] that will, in concert with other sensory modalities, supply the information stream at the bandwidth required to implement these new controllers on that machine.

We introduce a model for RHex's 4-bar legs [4] relating leg strain to leg kinematic configuration in the body coordinate frame. We compare against ground truth measurement the performance of the model operating on real-time leg strain data generated under completely realistic operating conditions. We introduce an algorithm for computing six degree of freedom body posture in world frame coordinates from the outputs of the six leg configuration models, together with a priori information about the ground. We discuss the manner in which such stance phase configuration estimates would be fused with other sensory data to develop the continuous time full body state estimates.

Figure 1: RHex with 4-bar legs in a natural setting.

Designed for simplicity, RHex has only one actuated degree of freedom per leg. In consequence, the legs cannot generally protract without stubbing the ground, and continuous locomotion requires their con-

*This work is supported by DARPA/SPAWAR Contract N66001-00-C-8026.

tinual recirculation. The strain measurements from the compliant members of the freely rotating 4-bar legs are obtained through a wireless high speed network, LegNet [1], which is also described briefly.

The organization of the paper is as follows. We start with a brief introduction to the 4-bar legs in Section 2 followed by a modeling discussion in Section 3 that introduces a polynomial representation of the empirical function relating strain measurement to leg configuration. Section 4 concerns the data collection and fitting procedures for computation of leg model. Model performance is demonstrated by emprical data. A body posture computation algorithm is explained in Section 5. Emprical data is presented to discuss its performance. Section 6 concludes with final remarks, a summary of contributions and future directions.

2 4-Bar Legs

The RHex 4-bar leg [4] illustrated in Figure 2 is a passive mechanical system composed of four parts: a hip clamp; front and rear compliant members; and a shin. The compliant members are thin rectangular fiber glass strips that are rigidly fixed at one end to the shin and connected to the hip clamp at the opposite end by a revolute joint (hinge) creating a 4-bar linkage structure on a plane which will be refer as the "leg plane" and denoted by $\mathcal{L} := \mathbb{R}^2$. The compliant parts are flexible in directions within the leg plane, $\mathcal{L}$, but "infinitely" stiff in other directions for all practical purposes. Combined with the constraints imposed by the closed chain mechanism the entire leg structure remains in the leg plane, $\mathcal{L}$, for all times. The hip clamp rigidly attaches this leg structure to the hip motor shaft such that the shaft axis is normal to the leg plane, $\mathcal{L}$, and goes through its origin.

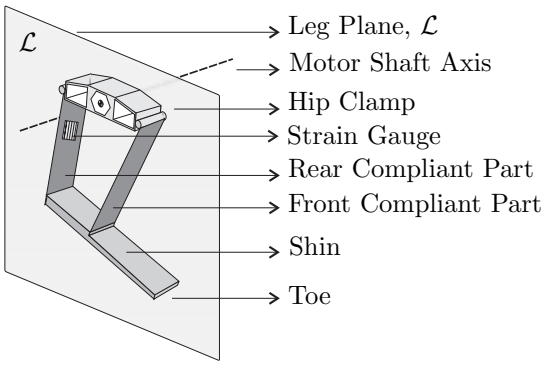

Figure 2: Key components of 4-bar leg mechanism.

A strain gauge (Vishay EA-250BK-10C) is installed onto the rear compliant part for measurement of strain, $\sigma \in \Sigma := \mathbb{R}^+$, which varies as a function of leg configuration. The gauge is located on the inside face near the hinge where strain is the smallest. In our emprical studies the maximum strain measured during tripod walking gait is approximately 1000 microstrain which falls within the 10^6 cycle at 1500 microstrain range reported in the strain gauge specifications[1].

RHex's freely rotating legs introduce a significant technical difficulty in taking measurements from sensors installed on them — this is essentially a "remote sensing" problem. In our implementation strain gauge measurements are transfered to the PC104 stack over a bi-directional digital wireless communication network, LegNet [1], featuring 50 Kbaud communication channel over a 916MHz carrier connecting a master located in the PC104 stack in the body to six self-contained embedded slave units mounted on each leg. In this setting we achieve synchronous sampling of all legs at 300Hz at 6-bit resolution.

3 Leg Model

We prefer to represent leg configuration in the clamp frame, $\mathcal{C} := \mathbb{R}^+ \times S^1$ — a polar coordinate system, attached to the hip clamp as depicted in Figure 3(b), whose states are the distance between hip attachment point and the toe, $l \in \mathbb{R}^+$, or "the effective leg length"; and, the angular deflection of toe vector from its rest position, $\delta \in S^1$.

Considering a quasi-static setting we ignore damping and leg mass and model the 4-bar leg as a pure passive spring attached to the hip clamp with torsional and radial compliance giving rise to a memoryless leg configuration model. Furthermore, since the locus of the physically valid toe positions, presented in Figure 4(left), has very small area we will consider 4-bar leg effectively as a 1-DOF mechanism. As a result, we define a scalar leg model mapping the strain, σ, to the polar coordinates of the toe, $\mathbf{c}$, given by a Taylor function, $\mathbf{m} : \Sigma \to \mathcal{C}$,

$$\mathbf{c} = \begin{bmatrix} l \\ \delta \end{bmatrix} = \mathbf{m}(\sigma) := \begin{bmatrix} \sum_{j=0}^{N} \left[n_j^1 . \sigma^j \right] \\ \sum_{j=0}^{N} \left[n_j^2 . \sigma^j \right] \end{bmatrix} \qquad (1)$$

[1] At a typical walking speed, the legs recirulate at roughly 2 Hz, hence we should expect mechanical sensor failures at a specified leg every 5 x 10^5 sec, hence, with six operating simultaneously, at some leg every 8 x 10^4 sec. Thus, at a typical a cruising speed of 1 m/s, we would expect to travel 80 km before suffering a leg sensor failure.

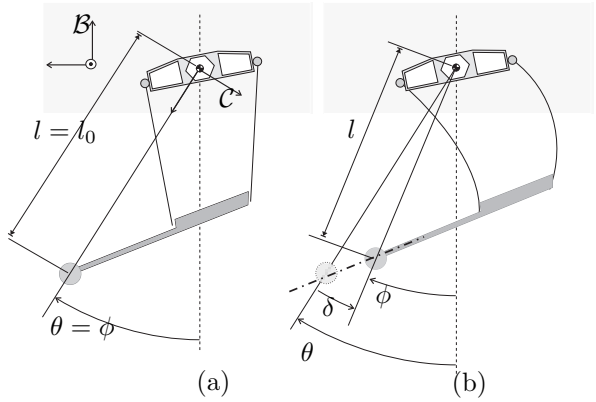

Figure 3: 4-bar leg (a) at rest and (b) during compression. Left sketch depicts two coordinate frames: the body frame, $\mathcal{B}$; and a clamp frame, $\mathcal{C}$. The right sketch illustrates the basic leg configuration variables, length, l, and deflection, δ, on a compressed leg. The dashed line depicts the approximate one dimensional locus of physically relevant toe positions.

where the length coefficients, $\{n_i^1 | i = 0, ..., N\}$, and deflection coefficients, $\{n_i^2 | i = 0, ..., N\}$, are computed by the fitting studies in Section 4.1.

4 System Identification

4.1 Data Collection and Model Fitting Study

A benchtop setup [3] is utilized to collect quasi-static leg data for modeling. This two degree of freedom setup allows the user to manually alter the configuration of an attached leg while recording the strain, σ, effective leg length, l, and leg deflection, δ, as well as the reaction force at the toe, $\mathbf{F}$.

The raw benchtop data set has an uneven distribution over the leg configuration space and contains configurations that cannot occur during locomotion. Therefore, prior to the fitting studies the raw data is avaraged out and evenly sampled, then filtered to pick those "physically relevant" points that correspond to ground contact with no slippage characterized by two conditions: 1) positive ground reaction force, $F_n > 0$; and 2) surface force that is less than the maximum Columb friction force, $F_s < F_c$. The maximum Columb friction force is given by $F_c = \mu F_n$ where F_n is the normal component of the ground reaction force, and μ is the friction coefficient which is emprically measured to be 0.5 for the 4-bar legs over card board paper. Figure 4(left) shows the scatter-plot of the set of physically relevant toe positions which forms a "thin" set — i.e., essentially a thinkened curve — in the leg plane, $\mathcal{L}$.

	Model Fit		Cross Validation	
Order	$p(l, \hat{l})$	$p(\delta, \hat{\delta})$	$p(l, \hat{l})$	$p(\delta, \hat{\delta})$
1	1.12%	4.87%	1.20%	5.44%
2	1.11%	4.79%	1.16%	5.51%
3	1.05%	4.53%	1.11%	5.19%
4	1.05%	4.43%	1.11%	5.26%

Table 1: Fitting and cross validation percentage normalized root mean square error for leg model in (1) at different polynomial orders. Small values indicate successful model prediction.

Figure 4(center) and Figure 4(right) illustrate scatter-plots of the effective leg length, l, and the deflection angle, δ, versus measured strain, σ, respectively. We compute the coefficients of the leg model in (1) by ordinary least squares. Letting $\hat{d}$ denote model prediction of a physical measurment, d, we measure model performance by the normalized root mean square error, $p(d, \hat{d})$, between the original data, d, and the corresponding model output, $\hat{d}$, given by

$$p(d, \hat{d}) := \sqrt{\frac{\left|\left|d - \hat{d}\right|\right|_2^2}{M(d_{\max})^2}} \times 100$$

where M is the length of the data vectors and $d_{\max}$ is the maximum value in original data.

Table 1 reports fitting and cross validation performances for the leg model in (1) with varying polynomial order, N. Since the improvement in model performance is insignificant for quadratic and higher order polynomials we choose to use the linear model due to its simplicity. Figure 4 also presents the best linear fits for the leg length, l, and deflection angle, δ.

4.2 Verification of Leg Model in Walking

In order to assess the performance of the linear leg model during walking we ran a set of experiments where the leg configuration as measured by a "ground truth" visual test station is compared with the leg model output. During these experiments we concentrate on a single leg whose motion is recorded by a high speed camera (RadLake HR-1000) at 125Hz and processed off-line to obtain ground truth leg configuration.

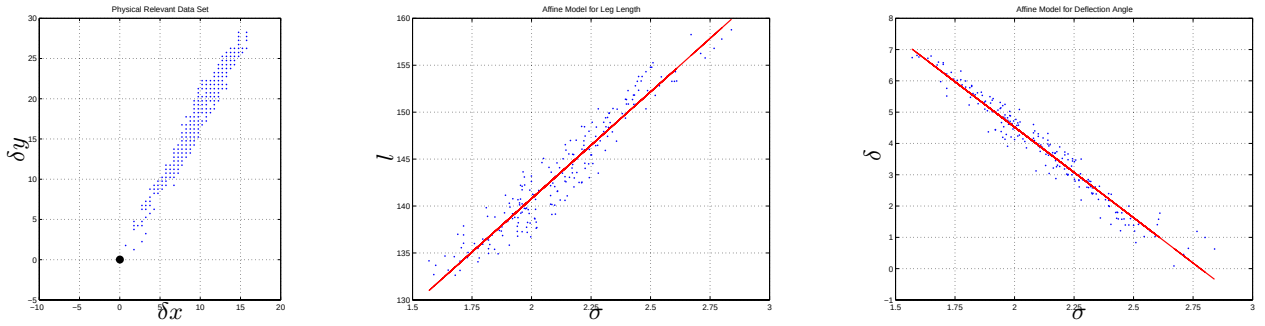

Figure 4: (Left) Scatter-plot of toe positions of the physically relevant cases. The axes of the plots are the cartesian displacement of the toe point, $(\delta x, \delta y)$, from the rest position which is indicated by the black circle. Resulting scatter-plots for leg length, l, (center) and deflection angle, δ, (right). The best fit line is depicted on both plots.

Speed	0.2 m/sec		0.45 m/sec	
	$p(l,\hat{l})$	$p(\delta,\hat{\delta})$	$p(l,\hat{l})$	$p(\delta,\hat{\delta})$
Exp #1	1.29%	10.34%	1.25%	15.00%
Exp #2	1.19%	7.77%	1.11%	16.95%
Exp #3	1.29%	8.77%	1.12%	12.01%
Exp #4	1.14%	6.38%	1.11%	12.97%
Exp #5	1.29%	8.89%	1.23%	9.61%

Table 2: Linear leg model performance during tripod walking measured by the percentage root mean square error between the model output and visually measured leg configuration. Small values indicate successful model prediction.

Figure 5 shows typical comparisons of the visually measured leg configuration states and the output of the leg model during a typical slow tripod walking gait (0.2 m/sec). The model performance for five runs at two different speeds can be found in Table 2 where the first two columns correspond to the plots in Figure 5.

5 Body Posture Computation

Define "tripod stride" to be a motion of the robot where the body is supported by three legs whose ground contact points (toes) are non-collinear and stationary (no slippage and no lift-off) for a time interval, $t \in [0, t_s]$. During a tripod stride the body frame, $\mathcal{B}$, is related to the world frame, $\mathcal{W}$, by a unique homogenous transformation which is parameterized by the configurations of the supporting legs.

Driven by this observation we introduce an on-line algorithm for 6-DOF body pose computation within a tripod stride in Section 5.1 followed by a discussion of preliminary verification studies in Section 5.2.

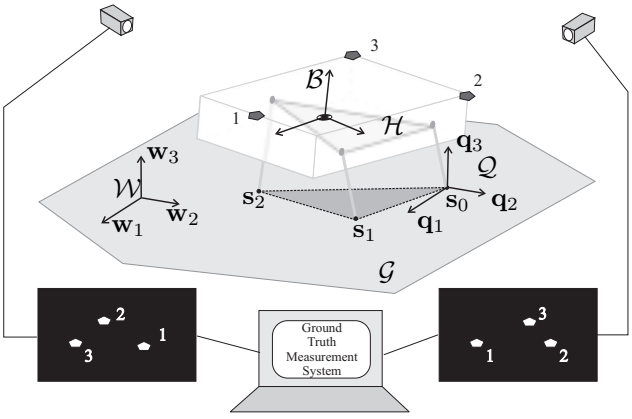

Figure 6: Robot supported on three legs on a flat ground surface, $\mathcal{G}$. Two cameras track three markers on the body which are depicted by numbered pentagons. An off-line system computes body pose with respect to the world coordinate frame, $\mathcal{W}$.

5.1 Computation of Body Pose within a Tripod Stride

Figure 6 illustrates a typical robot posture during a tripod stride. Without any loss of generality we will assume that supporting leg indices are $i = 0, 1, 2$. Using the leg model defined in (1) we compute the position of the i^{th} toe, $\mathbf{c}_i = \mathbf{m}(\sigma_i)$, in its associated hip clamp frame, $\mathcal{C}_i$, as a function of the strain across its compliant part, σ_i. The hip clamp frame, $\mathcal{C}_i$, is related to the body coordinate frame, $\mathcal{B}$, by a homogenous transformation, $\mathbf{h}_i^{\theta_i} : \mathcal{C}_i \rightarrow \mathcal{B}$, which is parametrized by the angular position of its hip shaft, θ_i. It directly follows

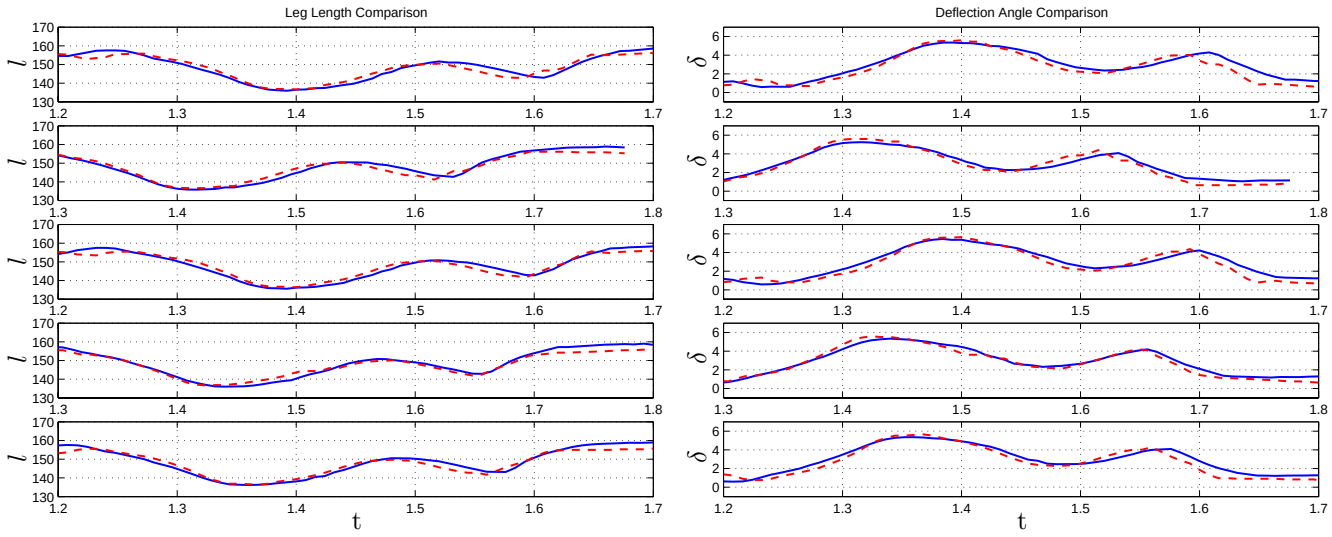

Figure 5: Comparison of visually measured (solid) and leg model generated (dashed) leg states during tripod walking at 0.2 m/sec. Plots from five runs for the effective leg length, l, (top) and deflection angle, δ, (bottom) are provided. Rows are ordered according to the experiment number to match with Table 2.

that the position of the i$^{\text{th}}$ toe in the body coordinate frame, $\mathbf{s}_i \in \mathcal{B}$, is given by $\mathbf{s}_i(\theta_i, \sigma_i) = \mathbf{h}_i^{\theta_i} \circ \mathbf{m}(\sigma_i)$.

Using the three ground contact points, $\mathbf{s}_i$, we define the support coordinate frame, $\mathcal{Q}$, centered at $\mathbf{s}_0$ with an orthonormal basis,

$$\begin{array}{lcl} \mathbf{q}_1 & := & \mathbf{e}_1, \\ \mathbf{q}_2 & := & \left[\mathbf{e}_2 - (\mathbf{q}_1^T \mathbf{e}_2)\mathbf{q}_1\right] / \left|\left|\mathbf{e}_2 - (\mathbf{q}_1^T \mathbf{e}_2)\mathbf{q}_1\right|\right|_2, \\ \mathbf{q}_3 & := & \mathbf{q}_1 \times \mathbf{q}_2, \end{array} \tag{2}$$

represented in the body frame, $\mathcal{B}$, where $\mathbf{e}_1 := (\mathbf{s}_1 - \mathbf{s}_0)/\left|\left|\mathbf{s}_1 - \mathbf{s}_0\right|\right|_2$ and $\mathbf{e}_2 := (\mathbf{s}_2 - \mathbf{s}_0)/\left|\left|\mathbf{s}_2 - \mathbf{s}_0\right|\right|_2$ are the unit vectors along the two edges of the support triangle. A homogenous coordinate transformation, $\mathbf{r} : \mathcal{B} \to \mathcal{Q}$, relates the body frame, $\mathcal{B}$, to this support frame, $\mathcal{Q}$,

$$\mathbf{r}(\mathbf{b}) := \mathbf{A}\mathbf{b} - \mathbf{A}\mathbf{s}_0, \tag{3}$$

where $\mathbf{A} := [\mathbf{q}_1\, \mathbf{q}_2\, \mathbf{q}_3]^T$.

The 6-DOF configuration of the body in the support frame, $\mathcal{Q}$, is composed of the position of the center of mass (COM),

$$\mathbf{u} := -\mathbf{A}\mathbf{s}_0, \tag{4}$$

and three rotational configurations: roll, γ; pitch, α; and yaw, β. The body lateral and fore/aft unity vectors in the world coordinates are $\mathbf{b}_1 = \mathbf{A}\,[1\,0\,0]^T$ and $\mathbf{b}_2 = \mathbf{A}\,[0\,1\,0]^T$, respectively. By direct computation we obtain the rotational configurations,

$$\begin{array}{l} \alpha := \arctan\left(\frac{\pi_3 \circ \mathbf{b}_1}{\sqrt{(\pi_1 \circ \mathbf{b}_1)^2 + (\pi_2 \circ \mathbf{b}_1)^2}}\right) \\ \gamma := \arctan\left(\frac{\pi_3 \circ \mathbf{b}_2}{\sqrt{(\pi_1 \circ \mathbf{b}_2)^2 + (\pi_2 \circ \mathbf{b}_2)^2}}\right) \\ \beta := \arctan\left(\frac{\pi_1 \circ \mathbf{b}_1}{\sqrt{(\pi_2 \circ \mathbf{b}_1)^2 + (\pi_3 \circ \mathbf{b}_1)^2}}\right), \end{array} \tag{5}$$

where we use the notation $\pi_i \circ \mathbf{f}$ to denote the i$^{\text{th}}$ entry of a vector, $\mathbf{f} \in \mathbb{R}^n$.

Note that during a stride the ground contacts remain stationary, hence, the support frame, $\mathcal{Q}$, is rigidly attached to the world coordinate frame, $\mathcal{W}$, and related by a homogenous transformation, $\mathbf{r} : \mathcal{Q} \to \mathcal{W}$, which can be specified by the inital pose of the the body at the begining of the stride.

5.2 Emprical Results

To assess the performance of the body pose computation algorithm on an operational robot we compare the ground truth measurements of the body pose to the output of this algorithm.

We attach three markers on the body denoting the body frame, $\mathcal{B}$, as illustrated in Figure 6. During locomotion a visual tracking system [7] logs the marker trajectories which are employed by an off-line process yielding 6-DOF body posture in world frame, $\mathcal{W}$.

Because the pose model represented in equations (4) and (5) is predicated upon the assumption that the robot is supported by a single tripod, it is important to

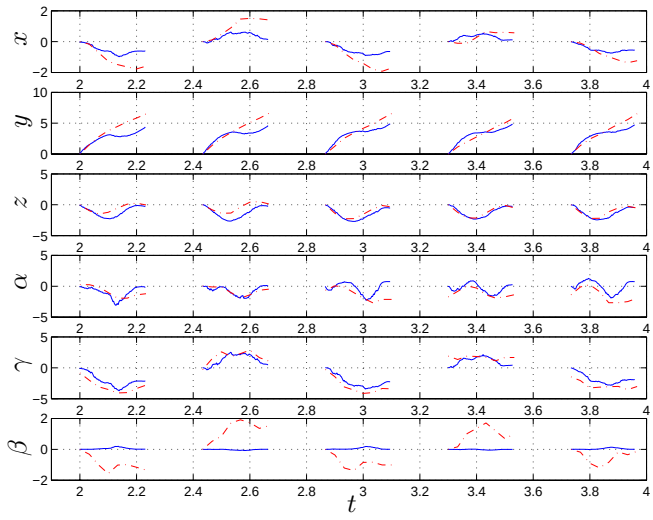

Figure 7: Pose states of the rigid body (solid) measured by GTMS and (dashed) computed according to our algoritm.

extract cues from the strain measurements that mark the onset and termination of the tripod stride. To this end, taking advantage of the assumption of a level support surface, we define a measure of co-planarity for all six legs, $\rho := \sum_{i=1}^{6} \mathbf{s}_i^T \mathbf{s}_i - \overline{\mathbf{s}}^T \overline{\mathbf{s}}$ where $\overline{\mathbf{s}} := 1/6 \sum_{i=1}^{6} \mathbf{s}_i$. Smaller values of ρ imply that all six toes are close to a common plane. In tripod walking small ρ values indicate double stance, and large values point out tripod support. We emprically pick a threshold, $\hat{\rho}$, to determine the start and the end of tripod support intervals. Figure 7 compares the body pose states obtained from ground truth measurement and output of pose computation algorithm showing very close match in most variables.

The reader should notice that the visual tracking system presently has a 5mm mean accuracy — coarse enough to jeopardize the accuracy of the angular state measurements. Furthermore, since both cameras of the tracking system look at the sagittal plane those states with significant component orthogonal to the sagittal plane, such as x displacement, have relatively higher error.

6 Conclusion

We have introduced a quasi-static leg model for a 4-bar linkage leg structure relating the strain in its rear compliant member to its configuration. Detailed emprical verification of the model both in benchtop experiments and in the normally functioning robot are presented where we demonstrated less than 2% error in leg length and less than 10% error in angular position of toe.

Based on the leg configuration model an algorithm for computation of robot posture during tripod support is introduced. Preliminary experimental data comparing its performance against ground truth measurements is presented.

In the near future we plan to fuse other sensory data streams such as 3-DOF laser rate gyros readings and visually registrated landmarks to build a full body state estimator mechanism with well characterized error margins. Such a technology will enable us to implement dynamical feedback controllers with significantly improved robustness and efficiency.

7 Acknowledgements

We thank Richard Groff for his careful contributions to the modeling effort and Gregory Sharp for his visual tracking system implementation. This work is supported by DARPA/SPAWAR Contract N66001-00-C-8026.

References

[1] H Komsuoglu. Legnet - a distributed wireless network. Technical report, University of Michigan, 2002.

[2] H. Komsuoglu, D. McMordie, U. Saranli, N. Moore, M. Buehler, and D. E. Koditschek. Proprioception based behavioral advances in a hexapod robot. In *International Conference on Robotics and Automation*, volume 4, pages 3650–3655, Seoul, Korea, 2001.

[3] P-C. Lin. Benchtop setting for compliant leg test and modeling. Technical report, University of Michigan, 2003. In preperation.

[4] E.Z Moore. Leg design and stair climbing control for the rhex robotic hexapod. Master's thesis, McGill University, November 2001.

[5] U. Saranli. *Dynamic Locomotion in a Hexapod Robot*. PhD thesis, Univerisity of Michigan, 2002.

[6] U. Saranli and D. E. Koditschek. Back flips with a hexapodal robot. In *IEEE International Conference on Robotics and Automation*, volume 3, pages 2209–2215, 2002.

[7] G. Sharp. Ground truth measurement system, 2003. http://sourceforge.net/projects/gtms/.

[8] Saranli U., M. Buehler, and D. E. Koditschek. Rhex - a simple and highly mobile hexapod robot. *International Journal of Robotics Research*, 20:616–631, 2001.

[9] Joel D. Weingarten, Martin Buehler, Richard E. Groff, and Daniel E. Koditschek. Automated gait generation and optimization for legged robots. 2003. In preperation.